HHS Public Access

Author manuscript

DNA Repair (Amst). Author manuscript; available in PMC 2023 January 01.

Published in final edited form as:

DNA Repair (Amst). 2022 January ; 109: 103247. doi:10.1016/j.dnarep.2021.103247.

Mouse embryonic fibroblasts isolated from Nthl1 D227Y knockin mice exhibit defective DNA repair and increased genome instability

Carolyn G. Marsden[1], **Lipsa Das**[4], **Timothy P. Nottoli**[2], **Scott D. Kathe**[1], **Sylvie Doublié**[1], **Susan S. Wallace**[1], **Joann B. Sweasy**[1,3,4,*]

[1]Department of Microbiology and Molecular Genetics, The Markey Center for Molecular Genetics, University of Vermont, Burlington, VT 05405-0068

[2]Section of Comparative Medicine, Yale University School of Medicine, New Haven, CT 06520, USA

[3]Department of Therapeutic Radiology, Yale University School of Medicine, New Haven, CT 06510

[4]Present address: Department of Cellular and Molecular Medicine, University of Arizona Cancer Center, Tucson, AZ 85724-5024, USA

Abstract

Oxidative DNA damage as a result of normal cellular metabolism, inflammation, or exposure to exogenous DNA damaging agents if left unrepaired, can result in genomic instability, a precursor to cancer and other diseases. Nth-like DNA glycosylase 1 (NTHL1) is an evolutionarily conserved bifunctional DNA glycosylase that primarily removes oxidized pyrimidine lesions. NTHL1 D239Y is a germline variant identified in both heterozygous and homozygous state in the human population. Here, we have generated a knockin mouse model carrying Nthl1 D227Y (mouse homologue of D239Y) using CRISPR-cas9 genome editing technology and investigated the cellular effects of the variant in the heterozygous (Y/+) and homozygous (Y/Y) state using murine embryonic fibroblasts. We identified a significant increase in double stranded breaks, genomic instability, replication stress and impaired proliferation in both the Nthl1 D227Y heterozygous Y/+ and homozygous mutant Y/Y MEFs. Importantly, we identified that the presence of the D227Y

[*]Corresponding author contact information: Department of Cellular and Molecular Medicine, University of Arizona Cancer Center, 1515 N Campbell Avenue, Tucson, AZ 85724-5024, USA, jsweasy@email.arizona.edu.

Author Statement

Carolyn Marsden: Methodology, Validation, Formal Analysis, Investigation, Writing-Original Draft, Visualization
Lipsa Das: Methodology, Investigation, Writing-Review and Editing
Timothy Nottoli: Methodology
Scott Kathe: Methodology, Investigation
Sylvie Doublié: Conceptualization, Writing-review and editing, Funding Acquisition
Susan Wallace: Writing-review and editing, Funding Acquisition
Joann Sweasy: Conceptualization, Supervision, Formal Analysis, Writing-review and editing, Funding Acquisition

Conflict of interest disclosure

The authors declare no conflict of interest.

variant interferes with repair by the WT protein, possibly by binding and shielding the lesions. The cellular phenotypes observed in D227Y mutant MEFs suggest that both the heterozygous and homozygous carriers of this NTHL1 germline mutation may be at increased risk for the development of DNA damage-associated diseases, including cancer.

Keywords

Base excision repair; NTHL1 glycosylase; oxidative DNA damage; genomic instability

1. Introduction

The survival of cells and organisms is dependent on the maintenance of genome integrity. DNA damage generated as a result of endogenous insults and exogenous agents can compromise genomic integrity if left unrepaired. Accumulation of DNA damage can potentially lead to cellular transformation, genomic instability and the development of human disease including cancer, premature aging, metabolic disorders, and neurodegenerative disease. Base excision repair (BER) is the predominant DNA repair pathway in cells responsible for the repair of non-bulky DNA base lesions which form the majority of endogenous DNA damage [1–5]. BER-mediated removal of a damaged nucleobase is a multistep process. The first step involves a DNA glycosylase locating a lesion and catalyzing the cleavage of the N-glycosyl bond between the base and 2'-deoxyribose generating an apurinic/apyrimidinic (AP) site [for review see [6]]. Bifunctional DNA glycosylases, which generally repair oxidatively-induced DNA lesions, possess both glycosylase and lyase activity. Therefore, bifunctional DNA glycosylases can potentially cleave the DNA backbone (utilizing their lyase activity) generating DNA ends that are further processed by AP endonuclease I (APE1) or polynucleotide kinase (PNK) [7–11]. Repair is completed after insertion of the missing base by DNA polymerase β (Pol β) and sealing of the nick by X-Ray Cross-Complimenting 1 (XRCC1) complexed with DNA ligase I or IIIα [for review see [12]]. Each step in the BER pathway is highly coordinated involving a number of protein-protein interactions, giving rise to reaction intermediates including abasic sites and single-stranded breaks which have the potential to be mutagenic and toxic [for review see [13, 14]]. Therefore, it is postulated that even subtle variations in specific proteins that participate in BER could result in mutagenesis and/or genomic stability.

NTHL1, the mammalian homolog of *Escherichia coli* endonuclease III, is an evolutionarily conserved bifunctional DNA glycosylase that functions in the initiation of BER [15–21]. NTHL1 removes a wide range of oxidized pyrimidine derivatives from DNA, including thymine glycol (Tg), 5-hydroxycytosine, 5-hydroxy-6-hydrothymine, 5,6-dihydroxycytosine, 5-hydrouracil, 5-formyluracil and formamidopyrimidines [15–18, 22]. Previous studies indicate that human NTHL1 functions as a housekeeping DNA glycosylase, scanning the DNA for oxidized pyrimidines [23]. Although NTHL1 is a ubiquitously expressed DNA glycosylase, differential mRNA expression in various tissues has been reported [23]. The highest NTHL1 mRNA levels detected by RT-PCR were found in oxygen-exposed lung whereas the lowest levels were detected in skeletal muscle [23]. These observations suggest that variants of NTHL1 that result in altered or defective function could

lead to tissue-specific phenotypes. Among various germline variants of NTHL1 identified in the human population, which are usually rare, D239Y is present in a heterozygous condition [21, 24, 25]. This variant has not yet been identified in human disease which may be attributed to its low frequency in the human population which limits statistical power in association studies. The highly conserved amino acid D239 is a catalytic residue within the active site of NTHL1. We have shown that this aspartate to tyrosine mutation generates an inactive glycosylase that still binds to DNA but cannot catalyze excision of the damaged base. When expressed in non-transformed human cells, D239Y NTHL1 leads to chromosomal aberrations, increased double-strand break formation, genomic instability and cellular transformation [25].

Despite NTHL1 being one of the most ubiquitous DNA glycosylases in eukaryotic cells, Nthl1 knock-out mice (*Nthl1*$^{-/-}$) were normal, long-lived, and fertile [26, 27]. Although *Nthl1*$^{-/-}$ mice did exhibit slower repair of Tg lesions in the liver after irradiation exposure and fragile telomeres in bone marrow cells proliferating in 20% oxygen, the observed repair impairment did not lead to overt phenotypes under unchallenged conditions [27]. The lack of phenotypes in *Nthl1*$^{-/-}$ mice indicated that redundancy in eukaryotic DNA glycosylases can compensate for the loss of Nthl1 [27]. In fact, most DNA glycosylase single-knockout mouse strains have been viable, fertile and exhibit a normal lifespan. The exceptions are thymine-DNA glycosylase (TDG) knockout mice, which are embryonic lethal, and uracil DNA-glycosylase knockout mice (UNG)$^{-/-}$ which exhibit a slight increase in spontaneous mutation frequency and increased incidence of B-cell lymphomas in mice over 18 months of age [for review see [28, 29]. However, double-knockout *Nthl1*$^{-/-}$/*Neil1*$^{-/-}$ mice exhibit a higher incidence of pulmonary and hepatocellular tumors compared to single-knockout strains, which may be associated with accumulation of 2,6-diamino-4-hydroxy-5-formamidopyrimidine (FapyGua) and 4,6-diamino-5-formamidopyrimidine (FapyAde) [30]. These results, in combination with the cellular phenotypes we observed in NTHL1 D239Y-expressing human cells, led us to hypothesize that mice harboring mutations in Nthl1 may exhibit more significant phenotypes than *Nthl1* knockout mice. We postulated that the back-up repair mechanisms that were compensatory in *Nthl1*$^{-/-}$ mice would not be activated in mice harboring a mutated Nthl1 and the dominant effects on BER would lead to more severe phenotypes in the mice.

To test our hypothesis, we have generated a knockin mouse model harboring Nthl1 D227Y mutation, (the amino acid in mice corresponding to human NTHL1 D239Y) and studied the DNA repair capacity and cellular phenotypes in mouse embryonic fibroblasts (MEFs). In this study, we found that the presence of a glycosylase-inactive variant D239Y NTHL1 significantly reduces the ability of WT to remove oxidized lesion, possibly by binding and blocking access to the lesion by the WT protein. MEFs heterozygous (Y/+) and homozygous (Y/Y) for the D227Y variant exhibited significant chromosomal aberrations and spontaneous and damage-induced γH2AX and 53BP1 foci. Finally, a concurrent replication stress, S-phase arrest and impaired cell proliferation was also observed in the D227Y mutants as compared to the WT MEFs.

2. Materials and methods

2.1. Generation and genotyping of Nthl1 D227Y knockin mouse

The Nthl1 D227Y knockin mouse model was generated using CRISPR/Cas9 by injecting Cas9 mRNA, a template oligonucleotide, and a single guide RNA (sgRNA) directly into mouse embryos, as generally described [31].

Guide RNA (gRNA) protospacer sequence:

GCCTTGTCTCCAAGCAGCAG

Nthl1HL1 D227Y template oligonucleotide:

ggacacagcccagctggcagagtgcccttggtcagcctgccttgtctccaagcagcagtg**Tac**acacatgtgcacagaatagcca accgactgaggtggaccaagaagatgaccaagaccc.

Cytoplasmic microinjection of approximately 250 embryos C57BL/6J was performed and the embryos were transferred to the uteri of pseudopregnant foster mothers. The F0 generation mice genotypes were analyzed by polymerase chain reaction (PCR) (see below) and sequencing the products. A single F0 male was backcrossed on a C57B1/6 background to generate F1 Nthl1 D227Y mice which was then also backcrossed on a C57B1/6 background. All MEFs in this study were isolated from F2 or higher generation heterozygous mating. Animals and MEFs were genotyped by polymerase chain reaction (PCR) analysis of tail DNA (DirectPCR, Viagen) using the following reaction conditions and cycling parameters:

Stock	Final
10X PCR_x Enhancer solution (ThermoFisher)	1X
10X Pfx amplification buffer (ThermoFisher)	1X
50 mM Magnesium sulfate (ThermoFisher)	1mM
10 mM dNTP mixture (New England Biolabs)	0.3mM each
10 μM Nth Forward and Reverse Primers: *Nth Forward primer*: 5'-GGAACTCACTTCACAGACC- 3' *Nth Reverse primer:* 5'-CCTGTGAGGGTAAGAGAAAGG- 3'	0.3 μM each
Platinum® Pfx DNA Polymerase (2.5U/ μL) (ThermoFisher)	1 U
Digested tail clipping solution	5 μL
Double-distilled, nuclease-free water (Invitrogen)	Up to 50 μL

Cycles	Temperature	Time
1	94°C	5 min
34	94°C 53°C	15 sec 30 sec

Cycles	Temperature	Time
	68°C	1 min
1	72°C	10 min
1	4°C	HOLD

To confirm that the Nthl1 PCR product (500 bp) was produced using the above PCR conditions, 3.5 μL of the PCR solution was combined with 6X DNA loading buffer (need recipe) and separated on a 1% agarose gel. 5 μL of the PCR solution was combined with 2 μL of ExoSAP-IT™ PCR Product Cleanup Reagent (ThermoFisher) and sequenced using Sanger sequencing.

2.2 MEF isolation and culture

Primary MEFs were isolated from 14.5-day embryos of Nthl1 Y/+ female bred with Nthl1 Y/+ male and cultured in Dulbecco's Modified Eagle Medium (DMEM) (Gibco) containing 10% fetal bovine serum (FBS) (Gibco) and 1 % penicillin-streptomycin (Gibco). MEFs were maintained at 37 °C in a humidified incubator in the presence of 5% oxygen, unless noted otherwise for experiments. MEFs at passage 5 or less were used in experiments.

2.3 Cell extract Tg excision assay

To prepare MEF cell extracts, MEFs were grown to 80% confluency then scraped in cold phosphate buffer saline (PBS). Collected cells were pelleted by centrifugation at 4°C for 5 min at 1250 rpm. The resultant pellet was resuspended in 5 packed cell volumes (PCV) of hypotonic lysis buffer [25 mM HEPES ((4-(2-hydroxyethyl)-1-piperazineethanesulfonic acid), 0.2 M EGTA ((ethylene glycol-bis(β-aminoethyl ether)-N,N,N′,N′-tetraacetic acid), 1.5 mM magnesium acetate ($MgOAc_2$), 10 mM potassium acetate (KOAc)] supplemented with 1 M dithiothreitol (DTT) and protease/phosphatase inhibitors (Roche), centrifuged at 1250 rpm for 5 min at 4°C. Cell pellets were resuspended in 3 PCV of hypotonic lysis buffer and allowed to swell on ice for 10 min then cells were lysed using a dounce homogenizer (22 strokes). Lysed cells were pelleted by centrifugation and resuspended in half-packed PCV of low salt buffer [25 mM HEPES, 0.2 M EGTA, 1.5 mM $MgOAc_2$, 10 mM KOAc, 25% glycerol]. Total protein concentration was calculated using the average of 2 prepared diluted samples read on a spectrophotometer.

An oligonucleotide (35 bases) with a centrally positioned Tg was 5′ end labeled with ^{32}P. The DNA substrate was made by labeling 1 pmol of the Tg-containing oligonucleotide with T4 polynucleotide kinase (New England Biolabs) and ATP-$\gamma^{32}P$ for 15 minutes at 37°C. The reaction was stopped by the addition of 1 mM EDTA and heating to 95°C for 1 minute. The DNA was ethanol precipitated and dried. The labeled oligo was annealed to a complimentary strand containing an adenosine opposite the Tg. 9 pmol of the unlabeled Tg-containing oligonucleotide was added along with 10 pmol of the complementary oligonucleotide in 10 mM Tris-HCl (pH 8.0) and 50 mM NaCl at a final concentration of 250 nM double-stranded oligonucleotide substrate. A non-radioactive 2 μM stock of Tg:A

was also made. The substrate was placed in a boiling water bath and cooled slowly to allow the DNA to anneal. The oligonucleotide sequences were as follows:

5’-TGTCAATAGCAAG[Tg]GGAGAAGTCAATCGTGAGTCT-3’ (damage-containing strand)

5’-AGACTCACGATTGACTTCTCCACTTGCTATTGACA-3’ (complementary strand)

Tg excision was assayed at 37 °C in 100 mmol/L NaCl, 25 mmol/L HEPES, pH 8.0, 2 mmol/L EDTA, and 100 μg/ml BSA. Reaction conditions were as follows: reactions with MEF cell extracts contained 5 nmol/L of Tg:A substrate/5μg cell extract; reaction with bacterially expressed NTHL1 contained 5 nmol/L of Tg:A substrate/20nM (active enzyme concentration) NTHL1; reaction with bacterially expressed NEIL1 contained 5 nmol/L of Tg:A substrate/80nM (active enzyme concentration) NEIL1. The reactions were quenched after 60 min in cold FE loading buffer [formamide (96 %), 20 mmol/L EDTA]. Substrate was separated from product using 12 % denaturing PAGE in TBE buffer. Bands were visualized and quantified using the Pharos FX plus Phosphoimager (BioRad). β-elimination and β,δ-elimination products were measured and the β-elimination product formation was graphed based on 3 independent experiments.

NTHL1 WT and D239Y variant were expressed from Rosetta 2 *Escherichia coli* cells via autoinduction and purified as described earlier[25], with the following modifications: after the His-Trap column (Cytiva), the protein was diluted to a final salt concentration of 150 mM NaCl and loaded onto a 5 ml Heparin HP column (Cytiva) equilibrated in heparin buffer (20 mM Tris-HC1, pH 8.0, 150 mM NaCl, 5 mM βME and 10% glycerol). The protein was eluted with a 20-column volume linear salt gradient (150 mM - 1M NaCl) in heparin buffer. Fractions were pooled and concentrated. The concentrated sample was loaded on a Superdex-200 gel filtration column (Cytiva) equilibrated in 20 mM Tris-HCl, pH 8.0, 100 mM NaCl, 5 mM βME, and 10% glycerol. Protein was pooled, aliquoted, flash frozen, and stored at −80°C.

Glycosylase and glycosylase/lyase assays contained a final concentration of 1,000 nM Tg:A substrate (20 nM radioactive, 980 nM nonradioactive), 10 mM Tris-HCl (pH 8), 75 mM NaCl, 1 mM DTT, and 2 mg/mL bovine serum albumin (BSA). The reactions were initiated by the addition of NTHL1 WT at a final concentration of 50 nM, NTHL1 WT, and NTHL1 D239Y at a final concentration of 50 nM each, and NTHL1 D239Y only at a final concentration of 100 nM. The assays were allowed to proceed at 37°C for 60 minutes. The glycosylase activity was determined by quenching half of the reaction in 0.1 N NaOH then heating in a boiling water bath for 5 minutes and adding an equal volume of formamide stop solution (98% formamide, 0.1 mM EDTA. 0.1% bromophenol blue and 0.1% xylene cyanol). The glycosylase/lyase activity was determined by quenching the other half with an equal volume of the formamide stop solution. The samples were resolved on a 12% polyacrylamide (w/v) sequencing gel, transferred to Whatman 3M paper, dried and exposed to a phosphor imager screen and imaged with a Pharos FX Plus Molecular Imaging System (BioRad). Results from three independent experiments were graphed.

2.4 Western blotting

MEFs were lysed in modified RIPA buffer (150 mmol/L NaCl, 50 mmol/L Tris pH 7.8, 1 % NP-40, 0.25 % sodium deoxycholate, protease and phosphatase inhibitors) then centrifuged at 10000xg for 10 min. Cleared cell lysates were combined with 6x loading buffer (375 mmol/L Tris-HCl, 9 % SDS, 50 % glycerol, bromophenol blue), separated on a 10 % SDS-PAGE gel and transferred to a polyvinylidene difluoride (PVDF-FL) membrane (Millipore). The membrane was blocked in Odyssey blocking buffer (Millipore) for 1 hr at room temperature (RT) with gentle shaking. The membrane was then probed with rabbit polyclonal NTHL1 primary antibody (1/1000) (Abcam) and mouse monoclonal tubulin primary antibody (1/10000) (Abcam, DM1A) overnight at 4 °C with gentle shaking. After 3 washes in PBS/0.1 % Tween, the membrane was probed with IRDye 800CW goat anti-mouse IgG (H+L) (1/20000) and IRDye 680RD goat anti-rabbit IgG (H+L) (1/20,000) for 1 hr at RT. The membrane was washed with PBS/0.1 % Tween and visualized using an Odyssey CLx Infrared Imaging System.

2.5 CHK1 S345 western blot assays

MEFs were plated at 2 x 10^5 per 60 mm plate and cultured under hypoxic conditions (5% O_2). Upon reaching 80% confluency, MEFs were treated with 50 μM menadione for 1 hr in the incubator (5% O_2). MEFs were washed 3 times with PBS then complete growth medium was added to the plates and MEFs were returned to the incubator. At 5 min, 10 min, 30 min, 1 hr and 2 hr post-treatment with menadione MEFs were washed with PBS and lysed in modified RIPA (see above) containing protease and phosphatase inhibitors and the resultant lysate was cleared by centrifugation at 10000xg for 10 min. Cleared cell lysates were combined with 6x loading buffer (see above), separated on a 15 % SDS-PAGE gel, and transferred to a polyvinylidene difluoride (PVDF-FL) membrane (Millipore). The membrane was blocked in 5% BSA (w/v) diluted in TBS for 1 hr at RT with gentle shaking. The membrane was then probed in 5% BSA (w/v)/TBS/0.1% Tween with rabbit monoclonal CHK1 S345 primary antibody (1/1000) (Cell Signaling, 133D3) and mouse monoclonal tubulin primary antibody (1/10000) (Abcam, DM1A) overnight at 4 °C with gentle shaking. After 3 washes in TBS/0.1 % Tween, the membrane was probed with IRDye 800CW goat anti-mouse IgG (H+L) (1/20000) and IRDye 680RD goat anti-rabbit IgG (H+L) (1/20,000) for 1 hr at RT. The membrane was washed with TBS/0.1 % Tween and visualized using an Odyssey CLx Infrared Imaging System. For all time points (except 10 min for WT and 5 and 10 min for Y/+), values graphed represent 2 MEF lines per genotype.

2.6 Proliferation assay

MEFs were plated at 10^5 per well in triplicate in a 6 well plate and cultured under hypoxic conditions (5% O_2) or normoxic conditions (20% O_2). At various days post-plating, MEFs were trypsinized, diluted 1:1 in trypan blue (0.2% in PBS), and counted using a hemocytometer. The number of viable cells per ml was calculated. Values represent 4 independent experiments.

2.7 Immunofluorescence

MEFs were plated (5 x 10^4) in 8 well chamber slides (LabTek). For MEF samples treated with menadione, growth media was removed and media containing 25 μM menadione was added to all the wells except the untreated control wells. MEFs were incubated with 25 μM menadione for 1 hr in the incubator (5% O_2) then washed 3 times with PBS. Complete media without menadione was added to the wells and the MEFs were allowed to recover for the indicated time points. MEFs were washed 2 times with PBS then fixed (4 % formaldehyde, 0.02 % Triton X-100) for 15 min at RT. MEFs were rinsed with PBS then incubated with blocking/permeabilization solution (10% normal goat serum, 0.5% Triton X-100) for 1 hr with gentle shaking. The blocking/permeabilization solution was then replaced with blocking/permeabilization solution containing diluted primary antibody as follows; mouse monoclonal anti-phospho-Histone H2A.X (Ser139): 1/200 (Millipore, clone JBW301) or rabbit polyclonal anti-53B1: 1/500 (Novus, NB100-304) and incubated overnight at 4 °C with gentle shaking. The next day, MEFs were washed with PBS/0.5 % Triton X-100 followed by 2 washes with PBS. MEFs were then incubated with AlexaFluor 488 goat anti-mouse IgG (H+L) antibody (1/1000) (ThermoFisher) diluted in blocking/permeabilization solution for 1 h with gentle shaking. MEFs were washed with PBS/0.5% Triton X-100 followed by 2 washes with PBS then slides were mounted in Fluoroshield with DAPI (Sigma). MEFs were imaged using a Zeiss LSM 510 META confocal scanning laser microscope. The number of cells with >25 γH2AX foci or the number of cells with >10 53BP1 foci were counted. Results represent 3 independent experiments using at least 2 MEF cell lines of each genotype.

2.8 Sensitivity to DNA damaging agent (menadione)

MEFs were plated at 10^5 cells/ml per well in triplicate in a 6 well plate and cultured under hypoxic conditions (5% O_2). The next day, MEFs were treated with 0, 10, 25, 40 or 75 μM menadione for 1hr in the incubator (5% O_2). MEFs were washed 3 times with PBS then complete growth medium was added to the plates and MEFs were returned to the incubator. Live MEFs were counted 5 days later using trypan blue exclusion. Values graphed represent 4 independent experiments.

2.9 Chromosomal aberrations

Metaphase spreads were prepared as previously described [32]. Metaphase spreads were imaged under a 100x objective using an Olympus BX50 Light Microscope with QImaging Retiga 2000R digital camera and software. Slides were coded and chromosomal aberrations were scored. At least 200 cells per genotype were counted.

2.10 Replication stress assay

MEFs were pretreated with 25μM menadione for 1 hr at 5% O_2 and washed using growth media. Cells were incubated with 1mM 5-bromo-2'-deoxyuridine (BrdU) for 24 hr to allow replication and incorporation of the BrdU label in the DNA. Cells were then washed twice with growth media and the incorporated BrdU label was chased for 0 hr or 24 hr. The 0 hr chase samples were considered a measure of total BrdU label that was incorporated in the cells. Cells were then fixed using 2% formaldehyde for 10 min, treated with 50mM

ammonium chloride for 5 min and permeabilized using 0.2% Triton X-100 for 10 min. To allow antibody access to the incorporated BrdU, DNA hydrolysis was performed by incubating cells with 1N HCl for 10 min at 4°C followed by 1N HCl for 10 min at RT. Cells were washed with 0.2% Triton X-100, blocked in 2% BSA for 20 min and incubated with Alexa Fluor 488 conjugated anti-BrdU antibody (Biolegend) for 30 min. Cells were washed with PBS and mounted using DAPI containing Prolong antifade mounting agent (Invitrogen). Cells were imaged using a Deltavision deconvolution microscope. At least 20 fields of view were imaged per sample. Results were compiled from 3 independent experiments.

2.11 Flow cytometry

Cells were either untreated or treated with 25μM menadione for 1 hour and allowed to recover for up to 24 hours. Cells were harvested using trypsin and fixed in 70% ethanol overnight at 4°C. Cells were washed with PBS and incubated with propidium iodide (PI)/RNase Staining Solution (Cell Signaling Technologies, USA) for 4 hr. PI-labelled DNA content was measured using BD FACSAria II Flow Cytometer (Becton-Dickinson, Mountain View, CA). The flow profiles were analyzed using ModFit LT software (Verity Software House, USA) to determine the cell cycle distribution and graphed using GraphPad Prism Version 5.0 (GraphPad Software).

2.12 Statistical analysis

All results are expressed as the mean ± SEM. The one-way ANOVA or two-way ANOVA were performed with a post-hoc Bonferroni test using GraphPad Prism Version 5.0 (GraphPad Software). One-way ANOVA has been applied to Figures 2–4 and two-way ANOVA has been applied to Figures 5–7. P-values of *p<0.05, **p<0.01, ***p<0.001 and ****p<0.0001 were considered statistically significant.

3. Results

3.1 Generation of Nthl1 D227Y knockin mouse using CRISPR-cas9

The Nthl1 D227Y knockin mouse was generated at the Yale Genome Editing Center using CRISPR-cas9 editing. Sequencing of Nthl1 was performed to determine the genotypes of the generated mice. As shown in Fig. 1, chromatograms were analyzed to identify D227 (WT) D/Y227 (Y/+; heterozygous) and Y227 (Y/Y; homozygous) mice. One major concern with using CRISPR-cas9 targeting to generate the Nthl1 mouse knockin model is the known high frequency of off-target-induced mutations at sites other than the intended target site [33–36]. The sgRNA was designed to have the lowest frequency of predicted off-target sites in the genome in order to minimize potential off-target mutations. To confirm that mutations were not generated in off-target sites, we sequenced 4 predicted off-target exon sequences with the highest sequence homology with the target sequence of the sgRNA and confirmed that none of the potential off-target sites harbored mutations (data not shown). Therefore, we are confident that the phenotypes reported in this study are a result of the Nthl1 D227Ymutation and not an off-target mutation.

3.2 Nthl1 D227Y Y/Y MEFs are deficient in Tg excision activity

We previously showed that human NTHL1 D239Y (corresponding to mouse D227Y) is catalytically inactive despite being able to bind to DNA [25]. Therefore, we measured Tg excision activity of D227Y mutants using cell extracts prepared from WT, Y/+, and Y/Y MEFs. As expected, Tg excision was significantly reduced in Nthl1 D227Y Y/+ cell extracts resulting in 2.6nM of β-elimination product as compared to 4.7nM in the WT MEFs. Tg excision was not detectable in Nthl1 D227Y Y/Y cell extracts (Fig. 2A, B). Total Nthl1 protein levels in the cell extracts were unaffected as measured by western blot (Fig. 2C). Therefore, differences in Tg excision activity were not a result of differences in total Nthl1 protein levels in the extracts. These results confirm that Nthl1 D227Y is catalytically inactive and demonstrate that Nthl1 D227Y Y/Y MEFs do not express an active Nthl1 protein.

Next, we sought to determine if the presence of inactive D227Y Nthl1 interferes with glycosylase or lyase activity of WT Nthl1. For this, we used purified WT and D239Y (human homologue of D227Y) NTHL1 expressed in *E. coli.* First, we confirmed that the purified WT NTHL1 DNA glycosylase is active in contrast to the D239Y Nthl1 variant (Fig. 2D). Next, we performed a competition assay between WT and D239Y NTHL1 by mixing equimolar concentrations of WT and D239Y NTHL1 and quantifying glycosylase and lyase activities. In these reactions, 50nM WT protein yields over 600nM DNA glycosylase product and ~ 300 nM product resulting from a combination of the glycosylase and lyase activities of the enzyme. However, mixing of 50 nM D239Y with 50nM WT NTHL1 significantly diminishes both products (Fig. 2D). These results suggest that the presence of the variant can bind and shield lesions away from WT Nthl1 DNA glycosylase.

3.3 Increased endogenous DNA damage-induced foci in untreated Nthl1 D227Y Y/+ and Y/Y MEFs

To determine if Nthl1 D227Y MEFs exhibit increased DNA damage, we measured the levels of γH2AX and 53BP1 foci in MEFs unexposed to exogenous DNA damaging agents. Nuclei were scored for γH2AX foci with at least 5 foci or 25 foci or 53BP1 for at least 5 or 10 foci. As shown in Fig. 3, D227Y Y/+ and Y/Y MEFs exhibited increased levels of γH2AX foci (A, B) and 53BP1 foci (C, D) compared to WT MEFs. When the nuclei were analyzed for the presence of higher numbers of DNA damage foci indicated by the presence of at least 25 γH2AX foci or 10 53BP1 foci, a statistically significant difference was observed between Y/+ and Y/Y MEFs. Therefore, both D227Y mutant Y/+ and Y/Y MEFs exhibited significantly increased levels of endogenous DSBs compared with WT MEFs.

3.4 Nthl1 D227Y mutant Y/+ and Y/Y MEFs exhibit increased levels of chromosomal aberrations

Given that an increased frequency of DSBs was observed in the Y/+ and Y/Y MEFs, we asked whether genomic instability in the form of chromosomal aberrations was present in these cells. We analyzed metaphase spreads from each genotype. Nthl1 D227Y Y/Y MEFs exhibited significant increases in chromosome/chromatid breaks and fragments (Fig. 4C–F) and Y/+ MEFs exhibited a significant increase in fragments compared to WT cells; there were no significant differences in the numbers of breaks and fragments in Y/+ compared to

Y/Y cells (Fig. 4E, F). Although no statistically significant differences in the numbers of fusions were detected between WT, Y/+ and Y/Y MEFs (Fig. 4A, B), both Y/+ and Y/Y MEFs exhibited slightly higher levels of fusions than WT MEFs. These results demonstrate increased levels of genomic instability in primary Nthl1 D227Y Y/+ and Y/Y MEFs.

3.5 Nthl1 D227Y Y/+ and Y/Y MEFs exhibit increased DNA damage-induced foci and increased sensitivity to DNA damaging agent

Given the increased endogenous DNA damage in D227Y mutant MEFs, we hypothesized that Nthl1 D227Y mutant MEFs would be inefficient in resolving oxidatively-induced DNA damage. To test this hypothesis, we treated WT, Y/+ and Y/Y MEFs with menadione (a DNA damaging agent that generates oxidatively-induced lesions) and measured γH2AX and 53BP1 foci at various time points post-treatment. Menadione was chosen as an oxidative DNA damaging agent as it induces reactive oxygen species and the associated oxidant stress. As shown in Fig. 5, the levels of γH2AX (A, B) and 53BP1 (C, D) foci remain significantly higher in both D227Y Y/+ and Y/Y MEFs at 4 hr and 8 hr after menadione treatment. No significant difference is observed between Y/+ and Y/Y MEFs after 4hr or 8hr recovery post-menadione treatment. In contrast, Nthl1 WT MEFs begin to recover at 4 hr post-treatment with decreased numbers of DNA-damage induced foci (A-D).

Since unresolved DNA damage can lead to decreased cell survival, we tested whether Nthl1 D227Y mutant MEFs were more sensitive to menadione. Nthl1 D227Y WT, Y/+ and Y/Y MEFs were treated with 10-75 μM menadione, allowed to recover for 8 days and then live cells were counted using trypan blue exclusion. Significantly reduced cell survival was observed in D227Y Y/+ and Y/Y compared to WT MEFs at higher concentrations of menadione (Fig. 5E). These results indicate that Nthl1 D227Y Y/+ and Y/Y MEFs are more sensitive to oxidatively-induced DNA damage resulting in increased DNA damage foci formation and decreased cell survival.

3.6 Impaired proliferation in Nthl1 D227Y mutant Y/+ and Y/Y MEFs

Increased levels of DNA lesions and DSBs can induce replication stress and affect cell proliferation. Most cells of the human or mouse body are exposed to lower levels of oxygen ranging from 3-8% which is considered physiologically relevant. Increasing the oxygen concentration to 20% is known to significantly induce oxidative DNA damage in MEFs, limit replicative lifespan and impair proliferation [37]. Therefore, we measured proliferation in Nthl1 D227Y mutant and WT MEFs under physiologically relevant (5% O_2) and high oxygen (20% O_2) levels. Under hypoxic conditions, both Y/+ and Y/Y MEFs exhibited a markedly reduced rate of proliferation as compared to WT MEFs (Fig. 6A). Next, we cultured the MEFs in 20% O_2 to mimic the O_2 concentration in ambient air and constitute an oxygen rich environment to test whether resulting increased oxidatively-induced DNA damage would further impact proliferation. As shown in Fig. 6B, proliferation of Nthl1 D227Y Y/+ and Y/Y MEFs was severely impaired when cultured in higher levels of oxygen (20% O_2 or normoxic conditions). As expected, proliferation of WT MEFs was also impacted by the higher levels of O_2 however not as severely as Y/+ and Y/Y MEFs (Fig. 6B). These results demonstrate that proliferation of Y/+ and Y/Y MEFs is significantly compromised which is exacerbated when cultured in higher levels (20%) of O_2.

3.7. Increased expression of phosphorylated CHK1 S345 and replication stress in Y/+ and Y/Y D227Y MEFs

Unrepaired DNA lesions that block progression of the replication fork (such as Tg) could lead to increased DSBs, as observed in D227Y mutant MEFs. Replication stress and subsequent activation of cell cycle checkpoints could also lead to slower rates of proliferation. Therefore, we assessed replication stress in Nthl1 D227Y WT and mutant MEFs. As seen in Fig. 7A, B we detected significantly increased phosphorylation of CHK1 S345, an indicator of blocked DNA replication, in Nthl1 D227Y Y/+ and Y/Y MEFs at 2 hr post-treatment with menadione as compared to WT MEFs.

We further tested replication stress by a pulse-chase experiment with BrdU, a nucleotide analog. In principle, cells are pulse labelled with BrdU to allow incorporation into DNA and chased to assess the loss or dilution of the incorporated BrdU label resulting from active replication. After treating WT and Y/Y MEFs with menadione for 1 hr, cells were pulsed with BrdU for 24 hr and the incorporated label was chased for 0 hr or 24 hr. As seen in Fig. 7C, there was no difference in total amount of incorporated BrdU label (0 hr) in the WT and Y/Y MEFs. After a 24 hr chase, there was a 40% decrease in BrdU positive nuclei in the WT cells, which indicates the BrdU label was diluted due to active replication (Fig. 7C, D). However, the percent of BrdU positive nuclei in Y/Y MEFs had no significant change after 24 hr indicating that the cells were not replicating and hence maintained the incorporated BrdU label (Fig. 7C, D). These results indicate that following oxidative stress, replication is significantly impaired in the Y/Y MEFs.

Next, we characterized the cell cycle of the mutant and wild-type MEFs. Cells stained with propidium iodide were sorted using flow cytometry to measure the cell cycle distribution in G0/G1, S and G2/M phases. As seen in Fig. 7E, the percentage of Y/Y and Y/+ MEFs in S-phase was significantly higher than the WT MEFs. Upon treatment with the DNA damaging oxidative agent menadione, within 8 hours, there was a significant increase in the percentage WT, Y/+ and Y/Y cells in S-phase as compared to the untreated cells. When cells were allowed to recover for 24 hours, the percent WT MEFs in S-phase was reduced indicating that the S-phase arrest was reversed. In contrast, the percent of Y/+ and Y/Y cells arrested in S-phase increased markedly showing a statistically significant increase compared to the WT. A slight increase in the percentage of Y/+ and Y/Y cells in G2/M phase was observed but remained statistically insignificant. Taken together, these data indicate that oxidatively-induced DNA damage induces an S-phase arrest in Nthl1 D227Y Y/+ and Y/Y MEFs.

4. Discussion

The BER pathway primarily repairs DNA lesions induced by reactive oxygen and nitrogen species and also alkylation damage. Potential replication-blocking lesions such as Tg, if left unrepaired, can impact genome stability and cell viability [25]. In this study, we have generated a knockin mouse model of the human germline variant NTHL1 D239Y (Nthl1 D227 in mice) using CRISPR-cas9 technology and studied the resultant cellular phenotypes in MEFs isolated from WT, Y/+ and Y/Y embryos. MEFs derived from the D227Y mouse show impaired Tg excision activity with decreased Tg excision in the heterozygous

variant Y/+ and undetectable Tg excision in the homozygous variant Y/Y. Additionally, we demonstrate a significant increase in chromosomal aberrations, DNA damage foci induced by both endogenous and exogeneous insults, and impaired proliferation in Nthl1 D227Y mutant Y/+ and Y/Y MEFs as compared to WT MEFs. Finally, we have shown a significantly increased replication stress in Nthl1 D227Y Y/+ and Y/Y MEFs including a persistent CHK1 S345 phosphorylation, a known marker of replication blockage and cell cycle arrest in S-phase. Remarkably, in the heterozygous state, the D239Y variant interferes with the lesion repair by the wild-type glycosylase, ultimately resulting in increased levels of replication stress and genomic instability. Our results suggest that heterozygous carriers of the NTHL1 germline variant are likely to develop diseases that result from genomic instability, such as cancer.

We have shown impaired Tg excision in Nthl1 D227Y Y/+ and Y/Y MEF cell extracts, respectively. The accumulation of replication-blocking lesions, such as Tg, can result in replication fork collapse during DNA replication leading to increased DSBs. As shown in Fig. 4–5, Nthl1 D227Y Y/+ and Y/Y MEFs exhibited increased DSB formation as indicated by an increased γH2AX and 53BP1 foci. In addition to DSBs, an increase in γH2AX foci may indicate an accumulation of DNA damage response factors in response to single-stranded breaks, replication fork stress as well as activation of cell-cycle checkpoint related factors [38, 39]. Therefore, we propose that increased DSBs in mutant D227Y MEFs are likely a consequence of replication fork collapse due to collision with unrepaired replication-blocking lesions such as Tg. In support of this hypothesis, Nthl1 D227Y Y/+ and Y/Y MEFs exhibited persistent expression of CHK1 S345 after treatment with menadione. CHK1 is phosphorylated in response to DNA damage to induce S-phase delay in order to prevent the cells from entering G2/M with under-replicated DNA and/or persistent DNA damage [40, 41]. Accordingly, an increased cell cycle arrest in S-phase was observed. Treatment with menadione, which induces oxidative stress, similar to endogenous oxidants, significantly increased DSBs and S-phase arrest. Therefore, persistent expression of CHK1 S345 after treatment with menadione and S-phase arrest indicates unresolved replication stress in Y/+ and Y/Y MEFs.

Collectively, these results suggest that the presence of the Nthl1 variant can interfere with successful repair of lesions possibly by blocking compensatory repair activities of other DNA glycosylases. As seen in *Nthl1*$^{-/-}$ mice, back-up glycosylases like NEIL1 can compensate for the absence of functional Nthl1[26, 27]. However, the presence of an aberrantly functioning glycosylase is expected to be damaging as it may recognize and bind the lesion and block access to other back-up repair glycosylases and hence compromise repair. Our previous studies have shown that expression of the NEIL1 G83D (germline variant in NEIL1) resulted in genomic instability and cellular transformation despite the expression of the WT glycosylases as well as the presence of other DNA glycosylases with similar substrate specificity [25, 42]. Therefore, we hypothesized that the D227Y Nthl1 recognizes and potentially shields the lesion preventing repair by other functional glycosylases. Our mixing experiments (Fig. 2) support this hypothesis as in the presence of both the wild-type and D239Y variant lesion removal by the WT NTHL1 enzyme is significantly compromised. Accordingly, compared to the WT, the glycosylase activity is reduced to 50% in the presence of equimolar concentrations of WT and D239Y NTHL1,

further indicating that the D239Y NTHL1 interferes with the lesion repair by the WT. In our previous study, we demonstrated that D239Y has a similar binding affinity as WT NTHL1 to DNA containing thymine glycol, supporting our suggestion [25]. It is important to note that this is a human germline variant, the human homologue of D227Y, in the heterozygous state suggesting that the presence of this variant can potentially compromise DNA repair in these individuals.

The presence of unresolved lesions can cause significant replication fork failure and stress leading to cell cycle arrest in S-phase and impaired cell proliferation as observed in Nthl1 D227Y Y/+ and Y/Y MEFs when cultured in 20% O_2. Although 20% O_2 is considered the standard or “normoxic” when culturing most mouse and human cell lines *in vitro*, most cells in the body are only exposed to about 2-8% O_2 [43, 44]. High levels of O_2 will lead to increased generation of reactive oxygen species (ROS) and therefore oxidatively-induced DNA lesions. Therefore, it is likely that the significant decrease in proliferation in Nthll D227Y Y/+ and Y/Y MEFs as compared to WT MEFs is the result of deficient repair of oxidatively-induced DNA lesions by mutant D227Y generated by increased ROS in the cell. Moreover, it is intriguing that Y/+ and Y/Y MEFs did not show a difference in the percentages of cell survival under different concentrations of menadione. As seen in Fig. 5C, we observe that menadione-induced DNA damage persists after 8 hours of recovery in both Y/+ and Y/Y cells as compared to WT, with no significant differences between Y/+ and Y/Y cells. Moreover, both Y/+ and Y/Y MEFs exhibit similar levels of S-phase arrest. This suggests that following menadione treatment, DNA repair is severely impaired in Y/+ cells similar to Y/Y cells. It is important to acknowledge that the remarkable increase in genomic instability and replication stress in unchallenged MEFs may result in a possible genetic drift and phenotypic alterations in mice in subsequent future generations. Hence, we have cryopreserved mice from F0/F1 generations to ensure future studies in case such genetic drift arises. We note that these studies were performed using MEFs and there could be differences in the observed genomic instability in other cell types.

Unrepaired DNA damage and genomic instability have been associated with a number of human diseases. Our results suggest that individuals who carry the D239Y germline variant could be at an increased risk for developing cancer and other human diseases. The findings from ongoing and future investigations of phenotypes in the adult Nthl1 D227Y knockin mice provide more information regarding potential links between the D227Y germline variant and susceptibility to disease onset and progression.

5. Conclusion

We conclude that the presence of D239Y germline variant of NTHL1 significantly induces DNA damage, leading to chromosomal aberrations, replication stress and impaired cell proliferation. Importantly, the presence of the variant interferes with the repair of oxidized lesions by the WT glycosylase indicating that the heterozygous expression of this germline variant can result in significant genomic instability.

Acknowledgments

We thank April Averill for expressing and purifying the WT and D239Y NTHL1.

Funding

This work was supported by National Institutes of Health grant awarded by National Cancer Institute [P01 CA098993].

References

[1]. Barnes DE, Lindahl T, Repair and genetic consequences of endogenous DNA base damage in mammalian cells, Annual review of genetics, 38 (2004) 445–476.

[2]. Krokan HE, Nilsen H, Skorpen F, Otterlei M, Slupphaug G, Base excision repair of DNA in mammalian cells, FEBS letters, 476 (2000) 73–77. [PubMed: 10878254]

[3]. Mitra S, Izumi T, Boldogh I, Bhakat KK, Hill JW, Hazra TK, Choreography of oxidative damage repair in mammalian genomes, Free radical biology & medicine, 33 (2002) 15–28. [PubMed: 12086678]

[4]. Izumi T, Wiederhold LR, Roy G, Roy R, Jaiswal A, Bhakat KK, Mitra S, Hazra TK, Mammalian DNA base excision repair proteins: their interactions and role in repair of oxidative DNA damage, Toxicology, 193 (2003) 43–65. [PubMed: 14599767]

[5]. Fromme JC, Gregory LV, Base excision repair, Adv Protein Chem, 69 (2004) 1–41. [PubMed: 15588838]

[6]. Kim YJ, Wilson DM 3rd, Overview of base excision repair biochemistry, Curr Mol Pharmacol, 5 (2012) 3–13. [PubMed: 22122461]

[7]. Zharkov DO, Shoham G, Grollman AP, Structural characterization of the Fpg family of DNA glycosylases, DNA Repair (Amst), 2 (2003) 839–862. [PubMed: 12893082]

[8]. Bailly V, Verly WG, Escherichia coli endonuclease III is not an endonuclease but a beta-elimination catalyst, The Biochemical journal, 242 (1987) 565–572. [PubMed: 2439070]

[9]. Bailly V, Derydt M, Verly WG, Delta-elimination in the repair of AP (apurinic/apyrimidinic) sites in DNA, The Biochemical journal, 261 (1989) 707–713. [PubMed: 2529848]

[10]. Chen DS, Herman T, Demple B, Two distinct human DNA diesterases that hydrolyze 3'-blocking deoxyribose fragments from oxidized DNA, Nucleic acids research, 19 (1991) 5907–5914. [PubMed: 1719484]

[11]. Wiederhold L, Leppard JB, Kedar P, Karimi-Busheri F, Rasouli-Nia A, Weinfeld M, Tomkinson AE, Izumi T, Prasad R, Wilson SH, Mitra S, Hazra TK, AP endonuclease-independent DNA base excision repair in human cells, Molecular cell, 15 (2004) 209–220. [PubMed: 15260972]

[12]. Nemec AA, Wallace SS, Sweasy JB, Variant base excision repair proteins: contributors to genomic instability, Seminars in cancer biology, 20 (2010) 320–328. [PubMed: 20955798]

[13]. Wallace SS, Murphy DL, Sweasy JB, Base excision repair and cancer, Cancer letters, 327 (2012) 73–89. [PubMed: 22252118]

[14]. Almeida KH, Sobol RW, A unified view of base excision repair: lesion-dependent protein complexes regulated by post-translational modification, DNA Repair (Amst), 6 (2007) 695–711. [PubMed: 17337257]

[15]. Aspinwall R, Rothwell DG, Roldan-Arjona T, Anselmino C, Ward CJ, Cheadle JP, Sampson JR, Lindahl T, Harris PC, Hickson ID, Cloning and characterization of a functional human homolog of Escherichia coli endonuclease III, Proc Natl Acad Sci U S A, 94 (1997) 109–114. [PubMed: 8990169]

[16]. Hilbert TP, Chaung W, Boorstein RJ, Cunningham RP, Teebor GW, Cloning and expression of the cDNA encoding the human homologue of the DNA repair enzyme, Escherichia coli endonuclease III, J Biol Chem, 272 (1997) 6733–6740. [PubMed: 9045706]

[17]. Dizdaroglu M, Karahalil B, Sentüker S, Buckley TJ, Roldán-Arjona T, Excision of products of oxidative DNA base damage by human NTH1 protein, Biochemistry, 38 (1999) 243–246. [PubMed: 9890904]

[18]. Asagoshi K, Yamada T, Okada Y, Terato H, Ohyama Y, Seki S, Ide H, Recognition of formamidopyrimidine by Escherichia coli and mammalian thymine glycol glycosylases. Distinctive paired base effects and biological and mechanistic implications, J Biol Chem, 275 (2000) 24781–24786. [PubMed: 10827172]

[19]. Eide L, Luna L, Gustad EC, Henderson PT, Essigmann JM, Demple B, Seeberg E, Human endonuclease III acts preferentially on DNA damage opposite guanine residues in DNA, Biochemistry, 40 (2001) 6653–6659. [PubMed: 11380260]

[20]. Ikeda S, Biswas T, Roy R, Izumi T, Boldogh I, Kurosky A, Sarker AH, Seki S, Mitra S, Purification and characterization of human NTH1, a homolog of Escherichia coli endonuclease III. Direct identification of Lys-212 as the active nucleophilic residue, J Biol Chem, 273 (1998) 21585–21593. [PubMed: 9705289]

[21]. Das L, Quintana VG, Sweasy JB, NTHL1 in genomic integrity, aging and cancer, DNA Repair (Amst), 93 (2020) 102920. [PubMed: 33087284]

[22]. Izumi M, Qiu-Mei Z, Katsuhito K, Hiroshi S, Masashi T, Akira Y, Shuji Y, Identification of 5-formyluracil DNA glycosylase activity of human hNTH1 protein, Nucleic acids research, 30 (2002) 3443–3448. [PubMed: 12140329]

[23]. Sarker AH, Ikeda S, Nakano H, Terato H, Ide H, Imai K, Akiyama K, Tsutsui K, Bo Z, Kubo K, Yamamoto K, Yasui A, Yoshida MC, Seki S, Cloning and characterization of a mouse homologue (mNthl1) of Escherichia coli endonuclease III, J Mol Biol, 282 (1998) 761–774. [PubMed: 9743625]

[24]. Marsden CG, Dragon JA, Wallace SS, Sweasy JB, Base Excision Repair Variants in Cancer, Methods in enzymology, 591 (2017) 119–157. [PubMed: 28645367]

[25]. Galick HA, Kathe S, Liu M, Robey-Bond S, Kidane D, Wallace SS, Sweasy JB, Germline variant of human NTH1 DNA glycosylase induces genomic instability and cellular transformation, Proc Natl Acad Sci U S A, 110 (2013) 14314–14319. [PubMed: 23940330]

[26]. Masashi T, Shin-ichiro K, Tatsuya S, Rei H, Hiroshi I, Shogo I, Altaf HS, Shuji S, James ZX, Le XC, Michael W, Kumiko K, Jun-ichi M, Manja M, Jan HJH, Gijsbertus van der H, Akira Y, Altraf HS, Novel nuclear and mitochondrial glycosylases revealed by disruption of the mouse Nth1 gene encoding an endonuclease III homolog for repair of thymine glycols, EMBO J, 21 (2002) 3486–3493. [PubMed: 12093749]

[27]. Masashi T, Shin-Ichiro K, Kumiko K, Qiu-Mei Z, Shuji Y, Gijbertus T.J.v.d.H., Akira Y, A back-up glycosylase in Nth1 knock-out mice is a functional Nei (endonuclease VIII) homologue, J Biol Chem, 277 (2002) 42205–42213. [PubMed: 12200441]

[28]. Parsons JL, Elder RH, DNA N-glycosylase deficient mice: a tale of redundancy, Mutat Res, 531 (2003) 165–175. [PubMed: 14637253]

[29]. Nilsen H, Rosewell I, Robins P, Skjelbred CF, Andersen S, Slupphaug G, Daly G, Krokan HE, Lindahl T, Barnes DE, Uracil-DNA glycosylase (UNG)-deficient mice reveal a primary role of the enzyme during DNA replication, Molecular cell, 5 (2000) 1059–1065. [PubMed: 10912000]

[30]. Chan MK, Ocampo-Hafalla MT, Vartanian V, Jaruga P, Kirkali G, Koenig KL, Brown S, Lloyd RS, Dizdaroglu M, Teebor GW, Targeted deletion of the genes encoding NTH1 and NEIL1 DNA N-glycosylases reveals the existence of novel carcinogenic oxidative damage to DNA, DNA Repair (Amst), 8 (2009) 786–794. [PubMed: 19346169]

[31]. Price NL, Rotllan N, Zhang X, Canfran-Duque A, Nottoli T, Suarez Y, Fernandez-Hernando C, Specific Disruption of Abca1 Targeting Largely Mimics the Effects of miR-33 Knockout on Macrophage Cholesterol Efflux and Atherosclerotic Plaque Development, Circ Res 124 (2019) 874–880. [PubMed: 30707082]

[32]. Lang T, Dalal S, Chikova A, DiMaio D, Sweasy JB, The E295K DNA polymerase beta gastric cancer-associated variant interferes with base excision repair and induces cellular transformation, Molecular and cellular biology, 27 (2007) 5587–5596. [PubMed: 17526740]

[33]. Hsu PD, Scott DA, Weinstein JA, Ran FA, Konermann S, Agarwala V, Li Y, Fine EJ, Wu X, Shalem O, Cradick TJ, Marraffini LA, Bao G, Zhang F, DNA targeting specificity of RNA-guided Cas9 nucleases, Nat Biotechnol, 31 (2013) 827–832. [PubMed: 23873081]

[34]. Fu Y, Foden JA, Khayter C, Maeder ML, Reyon D, Joung JK, Sander JD, High-frequency off-target mutagenesis induced by CRISPR-Cas nucleases in human cells, Nat Biotechnol, 31 (2013) 822–826. [PubMed: 23792628]

[35]. Mali P, Aach J, Stranges PB, Esvelt KM, Moosburner M, Kosuri S, Yang L, Church GM, CAS9 transcriptional activators for target specificity screening and paired nickases for cooperative genome engineering, Nat Biotechnol, 31 (2013) 833–838. [PubMed: 23907171]

[36]. Pattanayak V, Lin S, Guilinger JP, Ma E, Doudna JA, Liu DR, High-throughput profiling of off-target DNA cleavage reveals RNA-programmed Cas9 nuclease specificity, Nat Biotechnol, 31 (2013) 839–843. [PubMed: 23934178]

[37]. Parrinello S, Samper E, Krtolica A, Goldstein J, Melov S, Campisi J, Oxygen sensitivity severely limits the replicative lifespan of murine fibroblasts, Nature cell biology, 5 (2003) 741–747. [PubMed: 12855956]

[38]. Podhorecka M, Skladanowski A, Bozko P, H2AX Phosphorylation: Its Role in DNA Damage Response and Cancer Therapy, Journal of nucleic acids, 2010 (2010).

[39]. Cleaver JE, gammaH2Ax: biomarker of damage or functional participant in DNA repair "all that glitters is not gold!", Photochemistry and photobiology, 87 (2011) 1230–1239. [PubMed: 21883247]

[40]. Cho SH, Toouli CD, Fujii GH, Crain C, Parry D, Chk1 is essential for tumor cell viability following activation of the replication checkpoint, Cell Cycle, 4 (2005) 131–139. [PubMed: 15539958]

[41]. Liu Q, Guntuku S, Cui XS, Matsuoka S, Cortez D, Tamai K, Luo G, Carattini-Rivera S, DeMayo F, Bradley A, Donehower LA, Elledge SJ, Chk1 is an essential kinase that is regulated by Atr and required for the G(2)/M DNA damage checkpoint, Genes Dev, 14 (2000) 1448–1459. [PubMed: 10859164]

[42]. Galick HA, Marsden CG, Kathe S, Dragon JA, Volk L, Nemec AA, Wallace SS, Prakash A, Doublie S, Sweasy JB, The NEIL1 G83D germline DNA glycosylase variant induces genomic instability and cellular transformation, Oncotarget, 8 (2017) 85883–85895. [PubMed: 29156764]

[43]. McKeown SR, Defining normoxia, physoxia and hypoxia in tumours-implications for treatment response, Br J Radiol, 87 (2014) 20130676. [PubMed: 24588669]

[44]. Al-Ani A, Toms D, Kondro D, Thundathil J, Yu Y, Ungrin M, Oxygenation in cell culture: Critical parameters for reproducibility are routinely not reported, PLoS One, 13 (2018) e0204269. [PubMed: 30325922]

Highlights

- Germline variants of DNA repair proteins may interfere with successful DNA repair.
- A germline variant of base excision repair protein Nthl1 is an inactive glycosylase.
- The D227Y Nthl1 variant interferes with lesion removal by the wild-type protein.
- Genomic instability is present in murine embryonic fibroblasts carrying the variant.
- The presence of the variant may increase the risk of DNA-damage associated diseases.

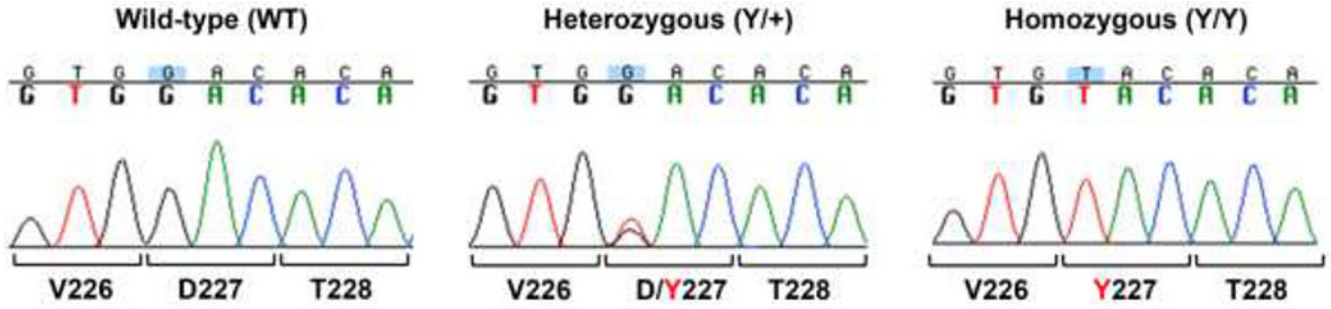

Fig. 1: Sequencing analysis of Nthl1 D227Y knockin mice.

Chromatograms of tail DNA sequences demonstrate generation of heterozygous (D/Y227: Y/+) and homozygous (Y227; Y/Y) mice using CRISPR-cas9 targeting.

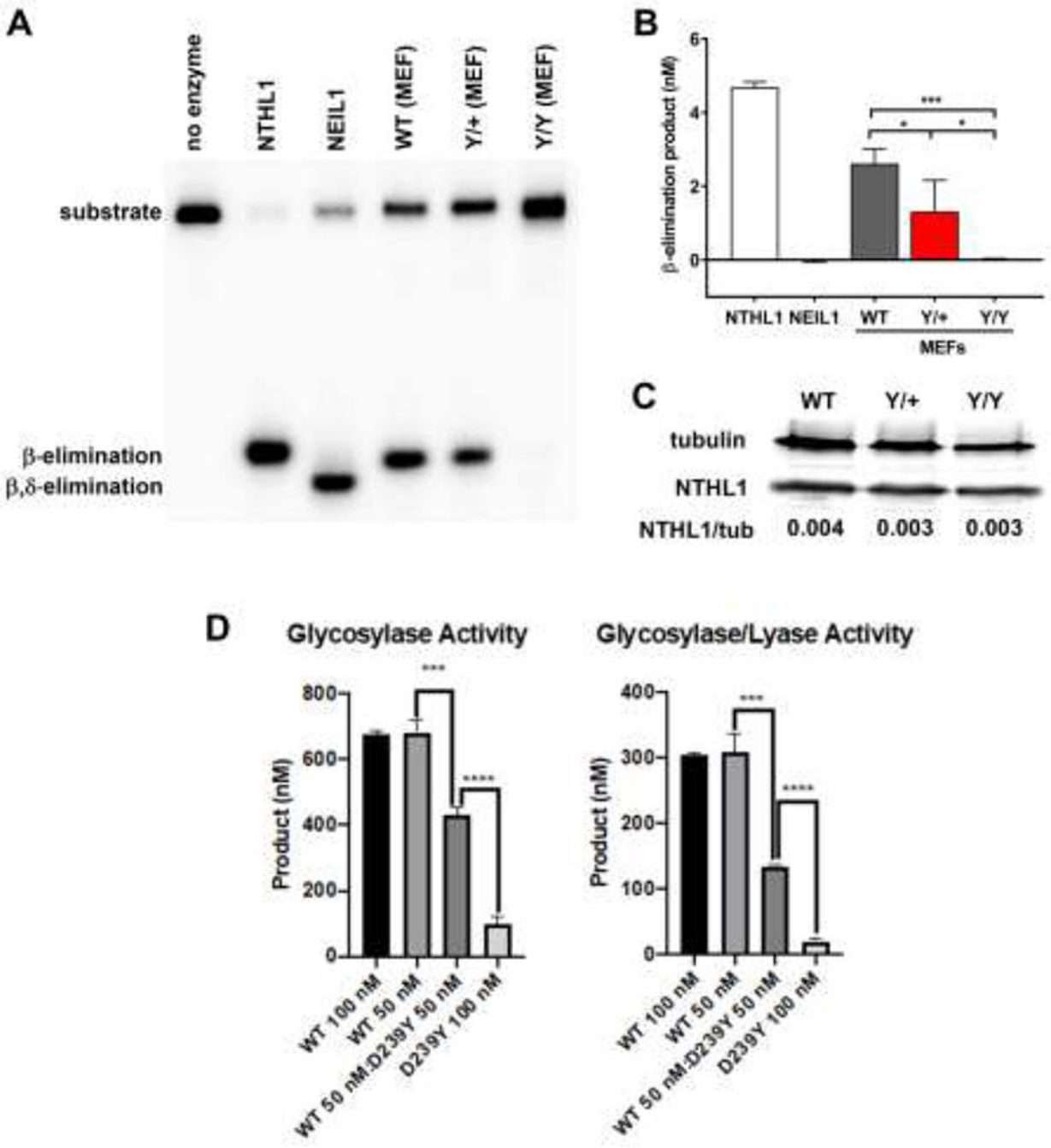

Fig. 2: No detectable Tg excision in Nthl1 D227Y Y/Y MEF cell extracts.

A. Excision activity of cell extracts (5μg) isolated from WT, Y/+ and Y/Y MEFs of a Tg lesion (5 nmol/L) after 60 min at 37°C. Purified NTHL1 and NEIL1 proteins expressed in bacteria are used as control. Excision activity is demonstrated by the formation of β-elimination or β,δ-elimination products **B**. β-elimination products relative to the substrate are graphed based on 3 independent experiments. One-way ANOVA and post-hoc Bonferroni test was used to determine statistical significance; *$p<0.05$, ***$p<0.001$. **C.**

Western blot demonstrates equivalent amounts of Nthl1 protein in cell extracts from WT, Y/+ and Y/Y MEFs. D.

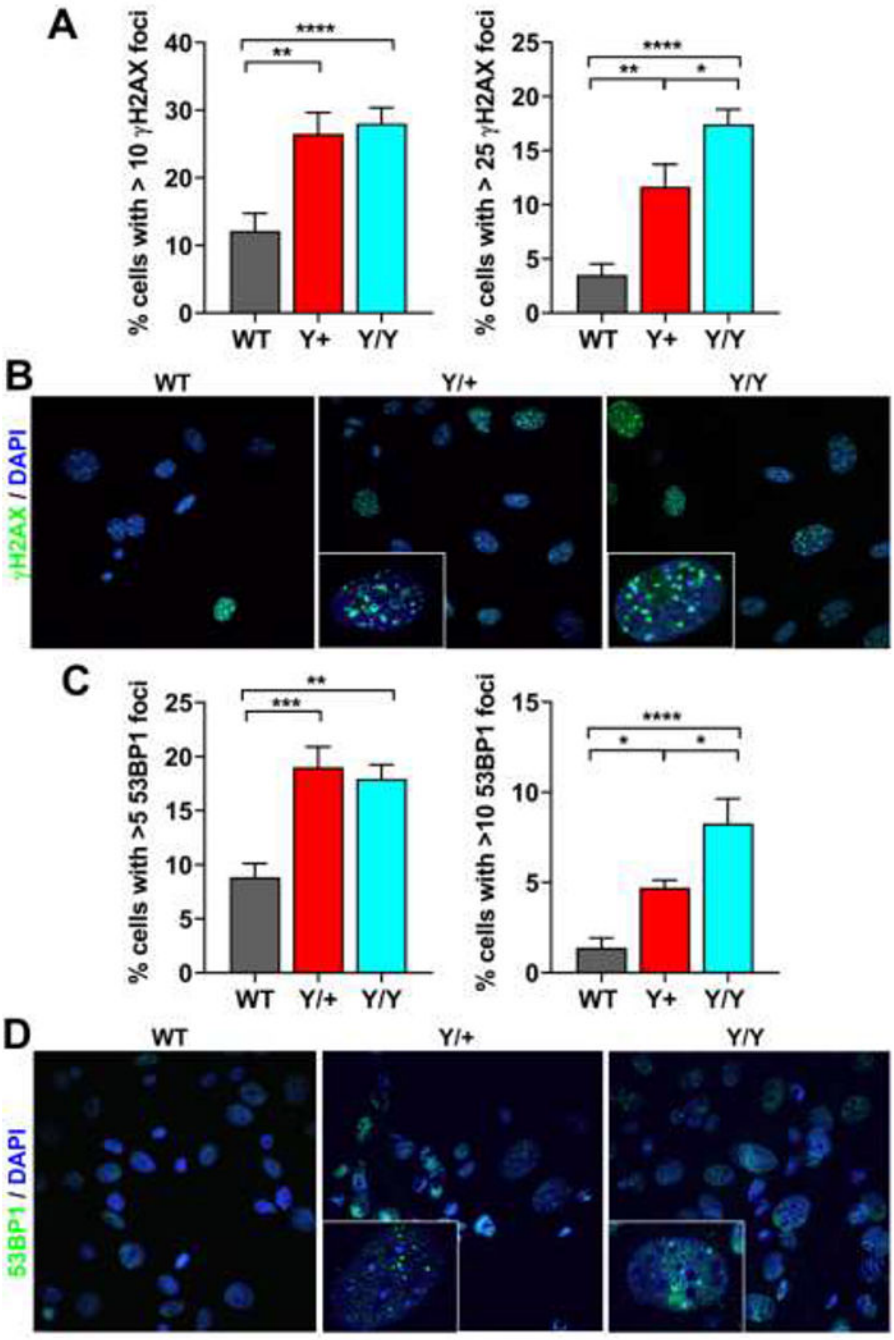

Fig. 3: Increased DNA damage-induced foci in untreated Nthl1 D227Y Y/+ and Y/Y MEFs.

Nthl1 D227Y MEFs were fixed and labeled with an antibody against γH2AX (A, B) or 53BP1 (C, D) (green) and mounted in Prolong Gold mounting media containing DAPI (blue, nuclei). Labeled cells were visualized using a Zeiss LSM 510 META confocal imaging system. **A, C.** Nuclei were scored for γH2AX foci with at least 5 or 25 foci or 53BP1 for at least 5 or 10 foci. The percentage of cells with nuclei containing greater than 10 or 25 γH2AX (A) or 5 or 10 53BP1 (C) foci are graphed as mean ± SEM. Statistical analysis was performed using one-way ANOVA and post-hoc Bonferroni test; *p<0.05, **p<0.01,

****p< 0.0001. **B, D.** Representative images of γH2AX (B) and 53BP1 (D) foci in Nthl1 D227Y WT, Y/+ and Y/Y MEFs. The insets show magnified images of a single nuclei.

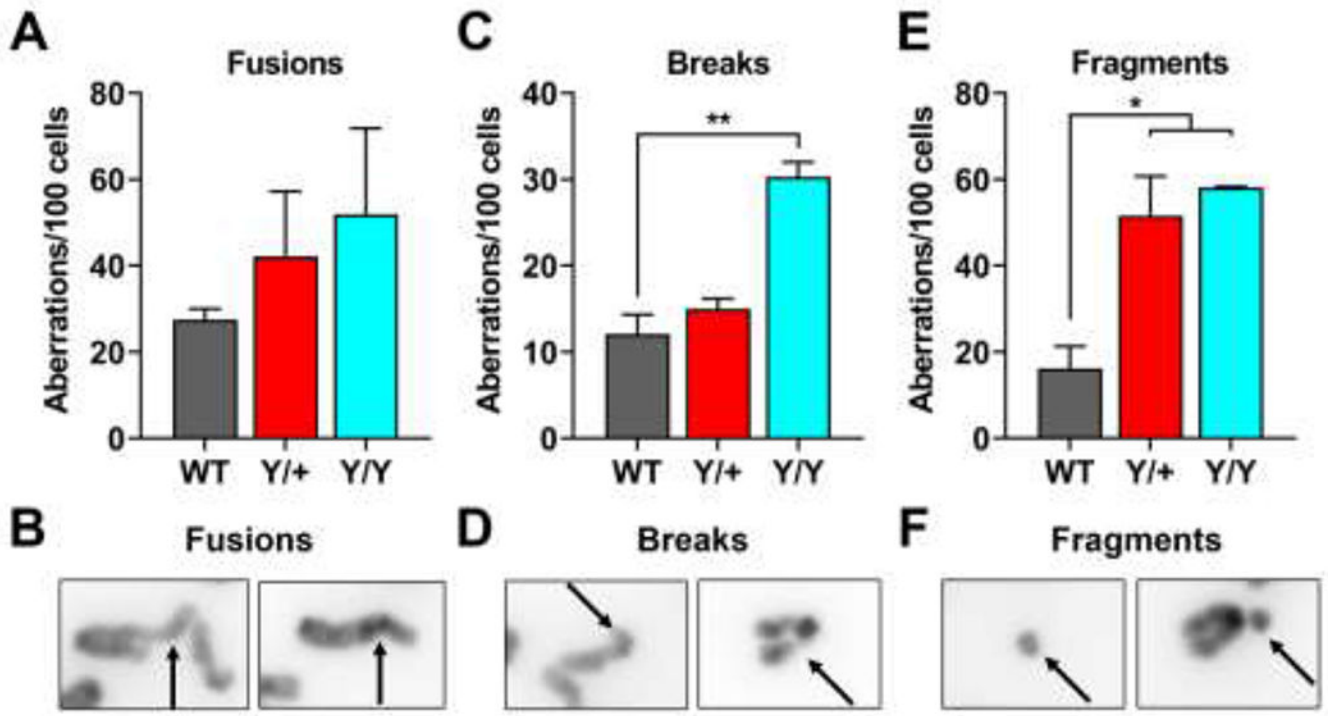

Fig. 4: Nthl1 D227Y Y/+ and Y/Y MEFs exhibit increased chromosomal aberrations.

Metaphase spreads were prepared from early passage WT, Y/+ and Y/Y D227Y MEFs. **A, C, E.** Column graphs showing the frequency of chromosomal aberrations e.g., fusions, breaks and fragments per 100 cells (mean ± SEM). Mutant Y/Y MEFs exhibit significantly increased levels of chromosomal breaks and both Y/+ and Y/Y MEFs exhibit significantly increased chromosomal fragments. One-way ANOVA and post-hoc Bonferroni test was used to determine statistical significance; *p<0.05, **p<0.01. **B, D, F.** Arrows point to examples of fusions (B), breaks (D) and fragments (F) observed in D227Y mutant MEFs.

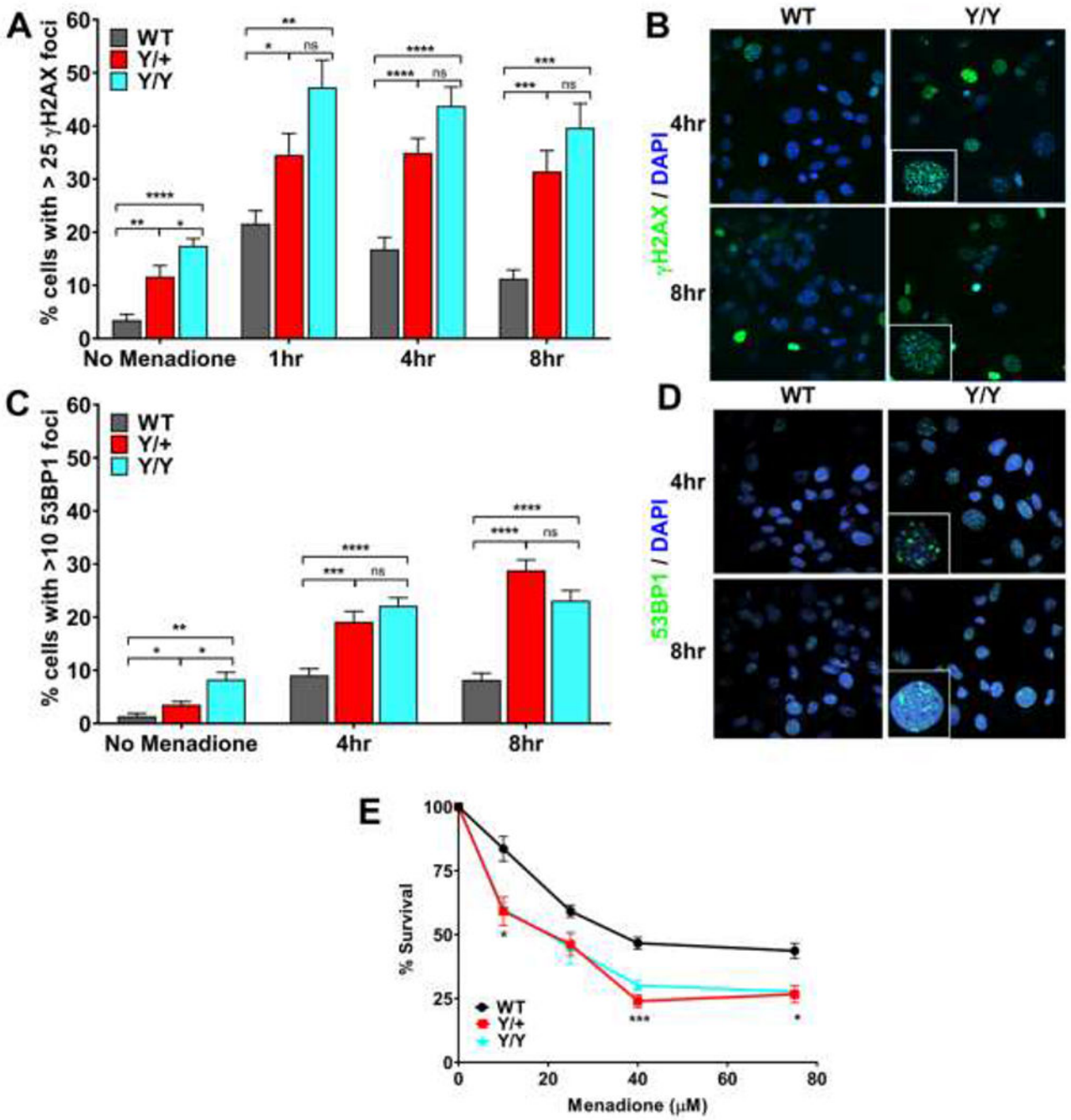

Fig. 5: Increased sensitivity to DNA damage in oxidatively-stressed D227Y Y/+ and Y/Y MEFs.

A-D. Nthl1 D227Y MEFs were either not treated or treated with 25 μM menadione for 1 hr. Cells were washed and allowed to recover for 1, 4 and 8 hr post-treatment. Cells were fixed and labeled with a γH2AX (A, B) or 53BP1 (C, D) antibody (green) then mounted in Prolong Gold mounting media containing DAPI (blue, nuclei). Labeled cells were visualized using a Zeiss LSM 510 META confocal imaging system. **A, C.** The percentage of cells with nuclei containing greater than 25 γH2AX (A) or 10 foci of 53BP1(C) were counted. The data are graphed as mean ± SEM. Two-way ANOVA and post-hoc Bonferroni test was

used to determine statistical significance; *p<0.05, **p0.01, ***p<0.001, ****p< 0.0001, ns, not significant. **B, D.** Representative images of γH2AX (B) and 53BP1 (D) foci in Nthl1 D227Y WT and Y/Y MEFs at 4 and 8 hr post-treatment (with expanded inset of a single nuclei in each graphed as mean ± SEM. Two-way ANOVA and post-hoc Bonferroni test was used to Y/Y image). **E.** Nthl1 D227Y MEFs were treated with 0, 10, 25, 40, or 75 μM menadione for 1 hr then washed and allowed to recover in 5% O_2 for 8 days. Live cells were counted using trypan blue exclusion. Percent cell survival is graphed and analyzed using two-way ANOVA and post-hoc Bonferroni test to determine statistical significance. *p<0.05, ***p<0.001.

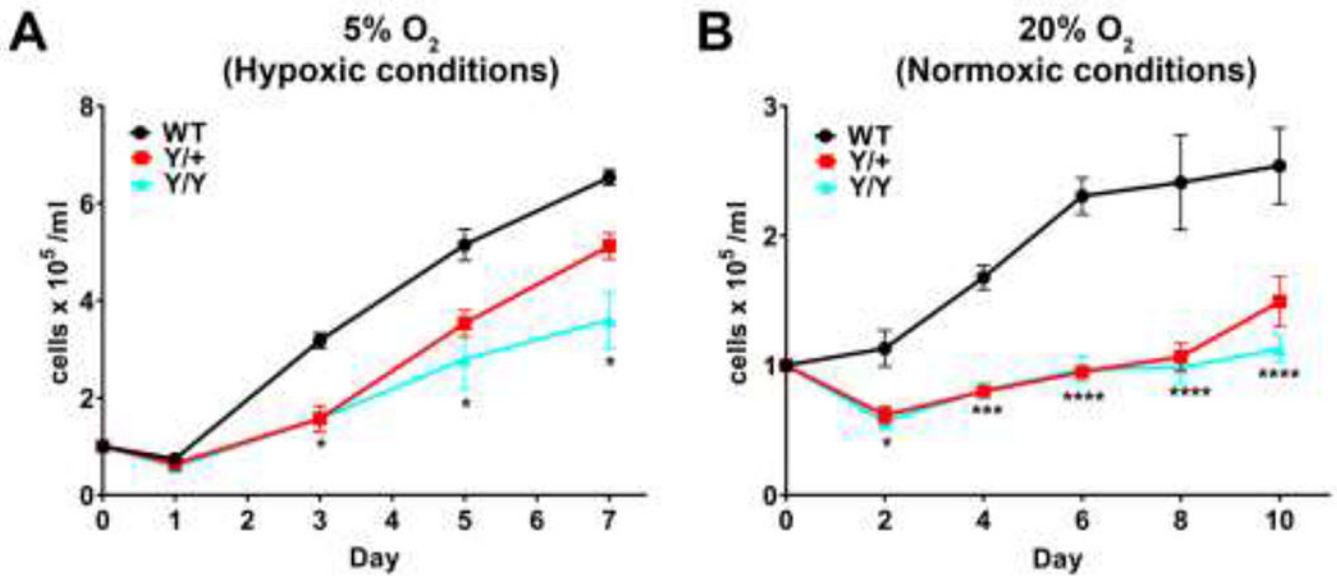

Fig. 6: Nthl1 D227Y Y/+ and Y/Y MEFs exhibit decreased proliferation.

Approximately 1 × 10^5 MEF cells under passage 1 were plated and grown under hypoxic (5%O_2) or normoxic (20%) conditions. Live cells were counted on indicated days using trypan blue exclusion. Data are graphed as cells x 10^5/ml ± SEM. **A.** Mutant Y/+ and Y/Y MEFs were found to grow slower compared to WT MEFs. **B.** Proliferation of each genotype was reduced under normoxic (20% O_2) conditions and significantly impaired in D227Y mutants Y/+ and Y/Y. Two-way ANOVA and post-hoc Bonferroni test was used to determine statistical significance; *p<0.05, **p<0.01.

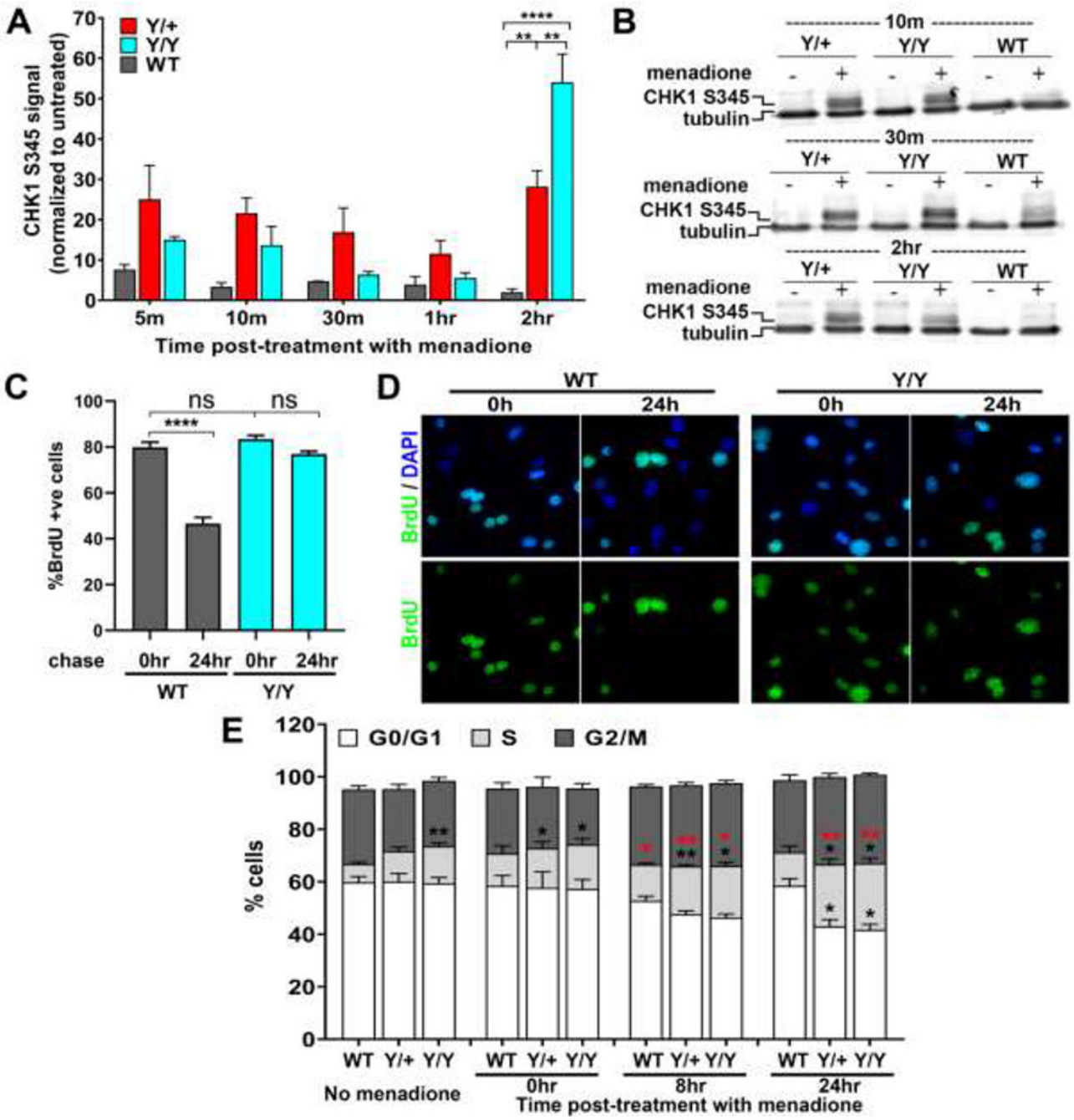

Fig. 7: Increased CHK1 S345 expression in D227Y Y/+ and Y/Y MEFs.

A. Quantification of levels of phosphorylated CHK1 (S345), normalized to α-tubulin, at indicated timepoints after treatment with menadione (50 μM). **B.** Representative western blots probed with anti-CHK1 S345 antibody demonstrating increased CHK1 S345 levels at 2 hr post-treatment with menadione. Two-way ANOVA and post-hoc Bonferroni test was used to determine significance; ** p<0.01, *** p< 0.0001. **C.** Cells were pre-treated with menadione (25 μM) for 1 hr and pulse labeled with BrdU for 24 hr to allow incorporation into the DNA. Cells were washed and the BrdU label were chased for 0 hr or 24 hr. The

percentage of BrdU positive cells are shown in the graph (mean ± SEM). Cells chased for 0hr indicates total percentage of cells that incorporated BrdU, which is similar in WT and Y/Y MEFs. After 24 hr of chase, the percentage of BrdU positive cells was significantly reduced in WT MEFs but was unaffected in the case of Y/Y MEFs. **D.** Representative images of cells stained with BrdU label (green) and nuclei (DAPI, blue) after 0 hr and 24 hr chase in WT and Y/Y MEFs. Results represent 3 independent experiments. Statistical analysis was performed using two-way ANOVA and post-hoc Bonferroni test; ****$p<$ 0.0001, ns, not significant. **E.** Cell cycle distribution of MEFs which were either untreated or treated with 25μM menadione and recovered for 8hr or 24 hr post-menadione treatment. Cells were labelled with propidium iodide and analyzed using flow cytometry. The percent of cells in G0/G1, S. and G2/M phase were measured and graphed. Results represent 3 independent experiments. Statistical analysis was performed using two-way ANOVA and post-hoc Bonferroni test; *$p<0.05$, **$p<$ 0.01, ns, not significant. Asterisks in black indicate statistical significance for specific cell cycle stage when Y/+ or Y/Y is compared to the WT under respective treatment conditions. Asterisk in red indicate statistical significance of the menadione treated samples as compared to the no menadione treated samples for respective genotypes.